JACS
JOURNAL OF THE AMERICAN CHEMICAL SOCIETY
Article
pubs.acs.org/JACS

Discovery of the Pt-Based Superconductor $LaPt_5As$

Masaya Fujioka,[*,†] Manabu Ishimaru,[‡] Taizo Shibuya,[§] Yoichi Kamihara,[⊥] Chihiro Tabata,[∥] Hiroshi Amitsuka,[∥] Akira Miura,[#] Masashi Tanaka,[⊗] Yoshihiko Takano,[⊗] Hideo Kaiju,[†] and Junji Nishii[†]

[†]Research Institute for Electronic Science, Hokkaido University, Sapporo, Hokkaido 001-0020, Japan
[‡]Department of Materials Science and Engineering, Kyushu Institute of Technology, Tobata, Kitakyushu, Fukuoka 804-8550, Japan
[§]IoT Devices Research Laboratories, NEC Corporation, Tsukuba, Ibaraki 305-8501, Japan
[⊥]Department of Applied Physics and Physico-Informatics, Faculty of Science and Technology, Keio University, Yokohama, Kanagawa 223-8522, Japan
[∥]Graduate School of Science, Hokkaido University, Sapporo, Hokkaido 060-0810, Japan
[#]Faculty of Engineering, Hokkaido University, Sapporo, Hokkaido 060-8628, Japan
[⊗]MANA, National Institute for Materials Science, 1-2-1 Sengen, Tsukuba, Ibaraki 305-0047, Japan

Supporting Information

ABSTRACT: A novel superconductor, $LaPt_5As$, which exhibits a new crystal structure was discovered by high-pressure synthesis using a Kawai-type apparatus. A superconducting transition temperature was observed at 2.6 K. Depending on the sintering pressure, $LaPt_5As$ has superconducting and non-superconducting phases with different crystal structures. A sintering pressure of around 10 GPa is effective to form single-phase superconducting $LaPt_5As$. This material has a very unique crystal structure with an extremely long c lattice parameter of over 60 Å and corner-sharing tetrahedrons composed of network-like Pt layers. Density functional theory calculations have suggested that the superconducting current flows through these Pt layers. Also, this unique layered structure characteristic of $LaPt_5As$ is thought to play a key role in the emergence of superconductivity. Furthermore, due to a stacking structure which makes up layers, various structural modifications for the $LaPt_5As$ family are conceivable. Since such a high-pressure synthesis using a Kawai-type apparatus is not common in the field of materials science, there is large room for further exploration of unknown phases which are induced by high pressure in various materials.

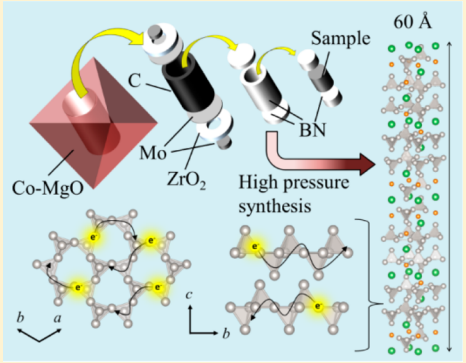

INTRODUCTION

There are few examples of superconducting Pt materials;[1] however, they have received remarkable attention for their unique properties.[2] In particular, the unconventional mechanism behind the Cooper pairing and the coexistence of superconductivity and magnetism have been widely discussed. For instance, the compounds with a heavy Fermion state (UPt_3),[3] non-centrosymmetric superconductors ($CePt_3Si$,[4] $BaPtSi_3$,[5] Li_2Pt_3B,[6] and $LaPt_3Si$[7]), a series of borocarbides RPt_2B_2C (R = Y, La, Pr, Nd, Th),[8−11] the recently discovered APt_3P (A = La, Ca, Sr),[12] and the quaternary Ca-Pt-Fe-As system[13−15] with a high superconducting transition temperature (T_c = 38 K) are under intense investigation. Yet, face-centered-cubic (fcc) Pt metal itself has not shown superconductivity, even at the lowest accessible temperature (T = 1.5 μK),[16,17] despite the fact that it has a high electronic specific-heat coefficient and a strong electron−phonon coupling, which are favorable conditions for superconductivity. Currently, it is generally agreed that spin fluctuations, which are ascribed to a large exchange interaction between the itinerant d electrons, compete with the phonon-mediated pairing in the noble transition elements like Pd or Pt. This idea is supported by several studies.[18−24] Such characteristics of Pt are considered to be one of the reasons why superconductors including Pt are much less well known. However, in the case of compacted sub-micrometer Pt particles, superconductivity was observed at 20 mK[25] due to the reduction of the spin fluctuations by spin−orbit scattering at the rough surface.[26−28]

In this research, we have defined "Pt-based superconductors" as superconductors where Pt is the main contributor to the electronic conductivity. In this regard, the quaternary Ca-Pt-Fe-As system is categorized as a Fe-based superconductor, because the superconducting layers are composed of Fe and As.[15] For $LaPt_5As$, Pt takes on the role of electron conductivity and forms corner-sharing tetrahedrons which spread out in the ab plane as a network-like layered structure. The unit cell shows an extremely long c axis (60.8 Å). A crystal structure such as this has not previously been reported.

Received: May 14, 2016
Published: July 27, 2016

DOI: 10.1021/jacs.6b04976
J. Am. Chem. Soc. 2016, 138, 9927−9934

In the research on superconductors, new crystal structures have provided important clues to the discovery of new superconducting families such as copper oxide,[29] iron-based,[30,31] and $BiCh_2$-based superconductors.[32,33] Each of these materials exhibits a layered structure, and various combinations of conducting and blocking layers have been conceived. $LaPt_5As$ also exhibits a layered Pt network structure, and conceivably the La or As site can be exchanged by other elements while retaining the Pt network. Thus, we can expect to obtain a series of new superconductors originating from $LaPt_5As$ as a base. $LaPt_5As$ cannot be synthesized without the use of high pressure, so the synthesis was carried out using a Kawai-type apparatus.[34] This can more effectively apply pressure to samples in comparison to a cubic-type apparatus.

The maximum pressure is primarily limited by the truncated edge length of the second-stage anvils; to apply higher pressure, sample size should be smaller. In the case of the cubic-type apparatus, studies were generally performed below 10 GPa. In this research, we successfully generated pressure up to 15 GPa using a Kawai-type apparatus and obtained single-phase superconducting $LaPt_5As$ at 10 GPa. With discovery of this $LaPt_5As$, there is large room for further exploration of new materials using pressures over 10 GPa. Such high-pressure synthesis is thought to be a promising method to develop various functional materials.

EXPERIMENTAL SECTION

Materials were prepared by high-pressure synthesis using a Kawai-type apparatus. La, Pt, and As powders were mixed with an elemental composition of La:Pt:As = 1:5:1, compressed into pellets, and sealed in an evacuated quartz tube. They are sintered at 500 °C for 10 h to obtain the precursors. The precursor was ground using mortar and pestle, and re-pelletized. In the Kawai-type apparatus, a Co-doped MgO octahedron was used as the pressure medium. The cell assembly was composed of the sample, BN capsule, carbon heater, Mo disk, and Mo electrode, as shown in Figure 1. The samples were sintered at around 1000 °C for 1 h at various pressures (4, 5, 6, 10, and 15 GPa). The truncated edge length of the second-stage anvils was adopted as 8 mm for 4, 5, 6, and 10 GPa and as 4 mm for 15 GPa. Diffraction patterns for each resulting material were measured (Rigaku, miniFlex300).

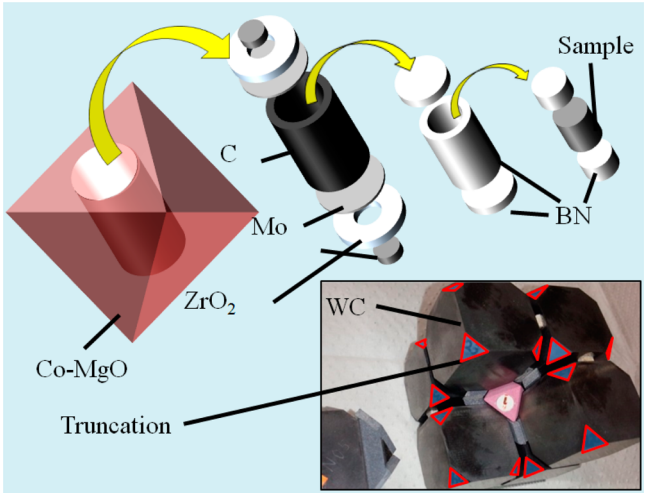

Figure 1. Schematic illustration of the Kawai-type cell assembly used in this study. Co-MgO, ZrO_2, Mo, C, and BN are used as the pressure medium, thermal insulator, electrode, heater, and separator of heater and sample, respectively. BN also works as a pressure medium. Inset shows the second-stage anvils and the inserted cell. These eight anvils composed of WC are pressed by six first-stage anvils. Truncations are highlighted.

To determine the detailed crystal structure, synchrotron X-ray powder diffraction (XRD) measurements were performed at room temperature at the BL02B2 experimental station of SPring-8 (JASRI; Proposal 2015A1441). The wavelength of the radiation beam was 0.49575(8) Å. The selected area electron diffraction (SAED) pattern and the convergent-beam electron diffraction (CBED) pattern were observed by transmission electron microscopy (TEM) (JEOL, JEM-3000F microscope). The initial structure model of this material was calculated by using the software Expo2014.[35] The detailed crystal structure was determined by Rietveld refinement.[36]

Magnetic measurements for the samples prepared under 4, 5, 6, 10, and 15 GPa were performed by using a superconducting quantum interference device (SQUID) magnetometer (Quantum Design, MPMS). The measurements were carried out under zero-field cooling and field cooling. Resistivity (ρ) measurements under magnetic fields (0, 0.1, 0.2, 0.4, 0.6, 0.8, and 1 T) and specific heat (C) measurements were also performed for samples synthesized under 10 GPa by a Physical Properties Measurement System (Quantum Design PPMS). To estimate the upper critical magnetic field (H_{c2}), the Werthamer–Helfand–Hohenberg (WHH) model was adopted.

The densities of states (DOSs) of $LaPt_5As$, $LaPt_2$, and $LaPt_5$ were obtained by density functional theory (DFT) within the generalized gradient approximation (PBE),[37] as implemented in the plane-wave code VASP.[38,39] The core–valence interaction was treated within the projector-augmented wave scheme. The calculated structures are consistent with the experimentally reported ones.[40,41] For $LaPt_5As$, the 84-atom hexagonal unit cell was reduced to a 28-atom triclinic primitive cell, which has lattice parameters of $a = b = 5.306$ Å, $c = 20.493$ Å, $\alpha = 90°$, $\beta = 97.439°$, and $\gamma = 120°$, using the ASE package.[42] A plane-wave cutoff of 400 eV was used, and the Brillouin zones of $LaPt_5As$, $LaPt_2$, and $LaPt_5$ were sampled by $9 \times 9 \times 2$, $6 \times 6 \times 6$, and $9 \times 9 \times 10$ Γ-centered Monkhorst–Pack k-point grids, respectively. It was checked that geometry optimazation led to slightly larger lattice constants but did not significantly alter the DOS.

RESULTS

$LaPt_5As$ cannot be obtained by a solid-state reaction method at ambient pressure due to the solid solubility limit of Pt. However, high-pressure synthesis is effective to generate a good reaction with the excess Pt. Also, according to the sintering pressure, $LaPt_5As$ shows the three different crystal structure types. Obtained materials after high-pressure synthesis are stable even at ambient pressure. Figure 2 shows the temperature dependence of magnetization and XRD patterns for the samples sintered under 4, 5, 6, 10, and 15 GPa.

Samples at 4 and 5 GPa show similar XRD patterns. However, superconductivity appears at 2.3 K in the sample at 5 GPa. This suggests that at 5 GPa superconducting $LaPt_5As$ is already starting to form. In fact, until 10 GPa, the diamagnetic susceptibility is gradually enhanced with increasing sintering pressure. However, the observed crystallinity of the sample at 6 GPa shows obvious deterioration. This is because an intermediate state appears during the crystal transition. At 10 GPa, the XRD profile sharpens again, and perfect diamagnetism was also observed due to the formation of single-phase superconducting $LaPt_5As$.[43] Further increases in sintering pressure up to 15 GPa brought about the disappearance of superconductivity resulting from the next structural transition. So $LaPt_5As$ can be roughly classified into three different phases. In this Article, we have termed them the 5 GPa phase (non-superconductivity), 10 GPa phase (superconductivity), and 15 GPa phase (non-superconductivity). Hereafter, we mainly focus on the superconducting $LaPt_5As$ (10 GPa phase). The crystal

DOI: 10.1021/jacs.6b04976
J. Am. Chem. Soc. 2016, 138, 9927–9934

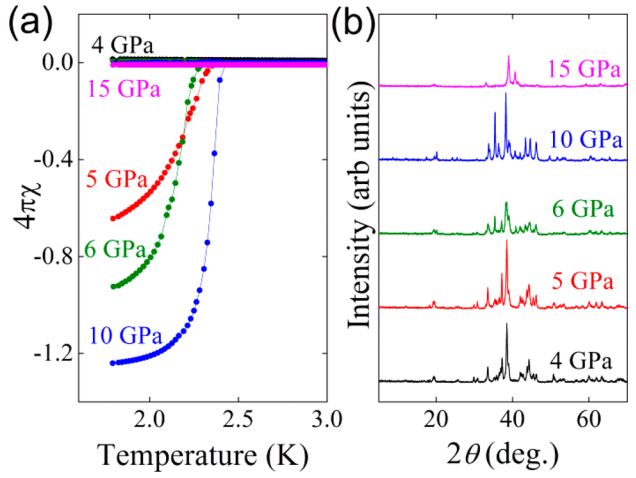

Figure 2. (a) Temperature dependence of magnetic susceptibility for $LaPt_5As$ sintered under various pressure (4, 5, 6, 10, and 15 GPa) from 1.8 to 3.0 K under 10 Oe. Demagnetization effects overestimate superconducting volume fractions in diamagnetic shielding measurements. (b) XRD patterns of $LaPt_5As$ for various sintering pressure (4, 5, 6, 10, and 15 GPa) in the 2θ range of 5−70°.

structure of the 10 GPa phase is successfully determined in this research. Figure 3 shows the result of the Rietveld refinements of the powder XRD pattern. First, through the analysis of electron diffraction patterns, the crystal system was found to be a hexagonal or rhombohedral system, and lattice parameters were roughly estimated to be a = 5.3 Å and c = 60.8 Å. A point group was then also determined by CBED analysis. The extinction rule of SAED suggested either $R\bar{3}c$ or $R3c$ as the candidates for the space group. These detailed analyses are shown in the Supporting Information (Figures S1 and S2). Based on these structural parameters, we extrapolated the initial structural models of 10 GPa phase using Expo2014 software. Each obtained initial structural model was checked against the Rietveld refinements, one by one, until the reliability factors of R_{wp} and S converged to appropriate value. As shown in Figure 3, although the residual errors corresponding to 00l reflections still exist because of its highly c-axis orientation, R_{wp} = 7.641 and S = 1.4398 were achieved. The structural parameters, including the Wyckoff position and atomic coordinates of each element, are described in Table 1. The inset of Figure 2 shows the DOSs obtained by DFT calculations based on these structural parameters. The projected DOSs for Pt were widely spread in the valence band region. In addition, the Fermi surface is almost occupied by the d orbitals of Pt. This suggests that the Pt contributes greatly to the electron conductivity.

Figure 4 shows the crystal structures and the high-resolution TEM image of the specimen synthesized at 10 GPa. $LaPt_5As$ has an extremely complicated crystal structure, as shown in Figure 4a. However, for the sake of clarity, it can be regarded that the structure is mainly composed of two different corner-sharing tetrahedrons, as shown in Figure 4b,c. The large tetrahedrons are composed of La and As and show three-dimensional corner-sharing. Further, La1 and As sites form two-dimensional layers, and the La2 and As sites form chains along the c axis to connect these La1−As layers. On the other hand, the nearest-neighbor Pt also consists of other corner-sharing tetrahedrons which stack along the c axis in layers. The hexagonal unit cell includes 12 Pt layers. The distances between the layers alternately enlarge and shrink, as shown in Figure 4c. Also La1−As layers are located in interlayer positions with larger distances.

In this material, there are three sites for Pt (Pt1, Pt2, and Pt3), and they form two slightly different sized Pt tetrahedrons. The Pt1 and Pt 3 sites are located at the vertex of the large and small tetrahedrons, respectively. The bottom face composed of the Pt2 sites is regular triangles and is parallel to the ab plane, as shown in Figure 4e. Each Pt−Pt length of the tetrahedrons is slightly smaller than the fcc Pt metal bond (2.77398 Å). In Figure 4d, each length and angle for the tetrahedron is described. Figure 4e shows the larger interlayer distance between the Pt layers. The Pt3 sites in the upper and lower layers are the closest to each other across the interlayer. Their distance is estimated to be 3.21944 Å, much longer than the Pt metal bond, whereas, in the smaller interlayers, the Pt1 and Pt2

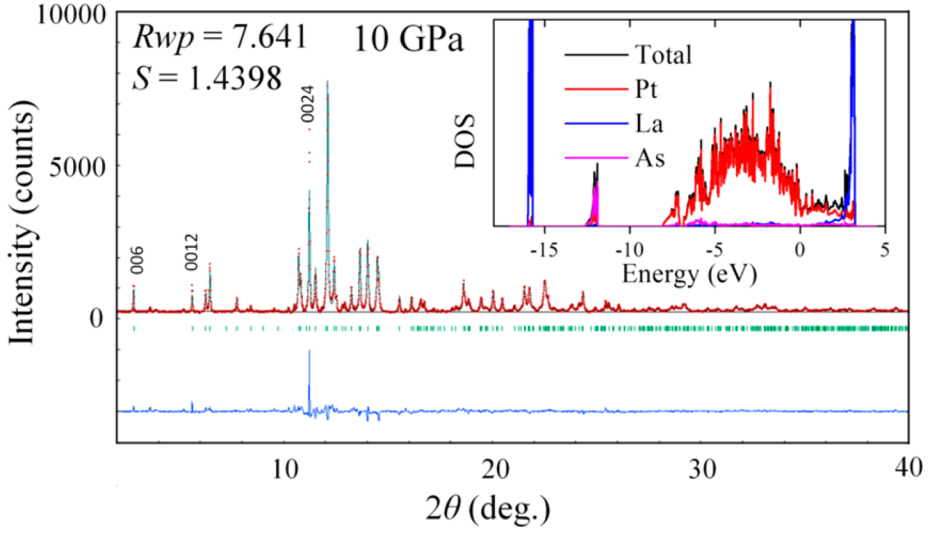

Figure 3. XRD pattern of superconducting $LaPt_5As$ with the result of the Rietveld refinement in the 2θ range of 2−40°. Described numbers are the Miller indices 00l. Red dots correspond to obtained data, the black lines are the calculated patterns, the blue lines are the difference between the calculated and obtained patterns, and the green bars correspond to the expected positions of Bragg reflections. Inset shows the DOS for $LaPt_5As$. The projected DOSs of Pt, La, and As are displayed by the red, blue, and purple lines, respectively.

DOI: 10.1021/jacs.6b04976
J. Am. Chem. Soc. 2016, 138, 9927−9934

Table 1. Structural Parameters of Superconducting $LaPt_5As$ Refined by Rietveld Analysis[a]

atom	Wyckoff position	SOF	x	y	z	B (Å^2)
La1	6*a*	1.0	2/3	1/3	1/12	1.38(15)
La2	6*b*	1.0	0	0	0	0.10(11)
Pt1	12*c*	1.0	0	0	0.09147(6)	1.40(7)
Pt2	12*c*	1.0	1/3	2/3	−0.00047(6)	0.83(7)
Pt3	36*f*	1.0	0.43310(34)	0.43242(36)	0.03778(3)	0.89(4)
As	12*c*	1.0	0	0	0.05127(12)	1.39(18)

[a]The space group is $R\bar{3}c$ (No. 167), Z = 12, a = 5.30633(17) Å, and c = 60.7864(14) Å. Site Occupancy Factors (SOF) are fixed at 1.0.

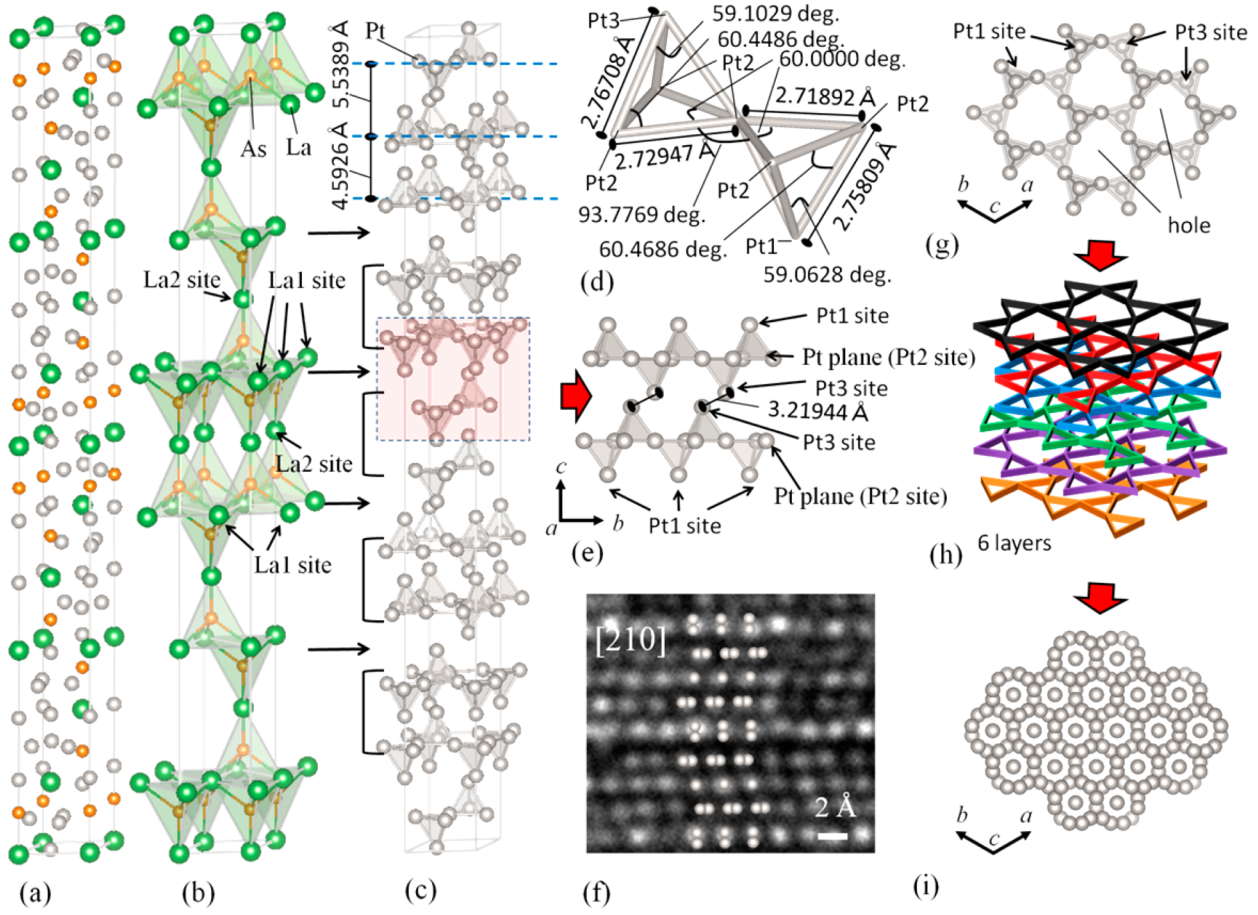

Figure 4. Schematic image of the crystal structure for new superconductor $LaPt_5As$. Green, silver, and orange circles indicate La, Pt, and As, respectively. (a) Unit cell of $LaPt_5As$. (b) Corner-sharing tetrahedrons composed of La and As. (c) Corner-sharing tetrahedrons composed of Pt. (d) Detailed information about Pt tetrahedrons. (e) Interspace in between Pt network layers. (f) High-resolution TEM image of $LaPt_5As$, viewed along the [210] direction. (g) Pt network structure spreading out in the *ab* plane. (h) Spirally stacked Pt network structure. (i) Projection of Pt in the *ab* plane.

sites show the closest positions across the interlayers. The length is 2.80882 Å, slightly longer than the Pt metal bond. In Figure 4g, the Pt layer on the *ab* plane is displayed. Upward tetrahedrons containing Pt1 sites and downward tetrahedrons containing Pt2 sites are alternately linked together and form the large hole enclosed in six Pt tetrahedrons. This network-like structure composed of Pt tetrahedrons spreads in the *ab* plane, and the above-described La2−As chains pass through the hole to connect with La1−As layers. Also since tetrahedrons are spirally rotated around their vertex along the *c* axis, the configuration in Figure 4i can be observed every six Pt network layers, as shown in Figure 4h. Incidentally, the result of X-ray photoelectron spectroscopy (XPS) measurement shows that the oxidation state of Pt in $LaPt_5As$ is nearly the same as that of metal Pt, as shown in the Supporting Information (Figure S3). Therefore, these Pt−Pt bonds are metallic in nature and play a major role in the flow of the superconducting current.

In addition, high-resolution TEM results are shown in Figure 4f. Since Pt is the heaviest element in this compound, the scattering from Pt is expected to be clearly observed. Actually, the bright spot in the TEM image agrees well with the Pt site in the schematic figure. To double-check the crystal structure, we calculated the electron diffraction pattern on the basis of the crystal structure obtained from the Rietveld refinements. Calculated electron diffraction patterns for the [210] and [110] faces are matched well with the observed electron diffraction patterns, as shown in the Supporting Information (Figure S2).

Figure 5a shows the temperature dependence of resistivity under magnetic field from 0 to 1 T for $LaPt_5As$. T_c is observed

DOI: 10.1021/jacs.6b04976
J. Am. Chem. Soc. 2016, 138, 9927−9934

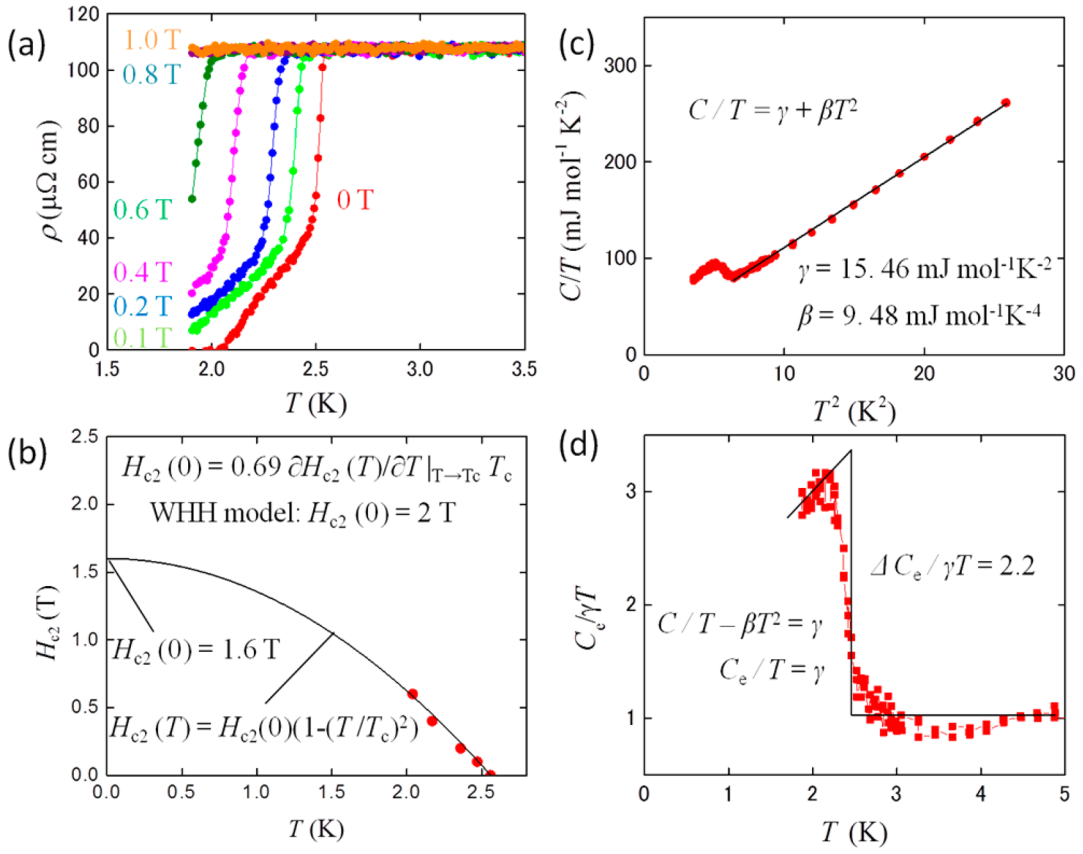

Figure 5. (a) ρ versus T from 1.8 to 3.5 K under magnetic field (0, 0.2, 0.4, 0.6, 0.8, and 1 T). (b) H_{c2} versus T with the simple phenomenological expression described by black line. (c) C/T versus T^2. Black line indicates the linear approximation in normal conducting state of $LaPt_5As$. (d) $C_e/\gamma T$ versus T. Black line shows the specific heat jump at T_c as a guide for the eye.

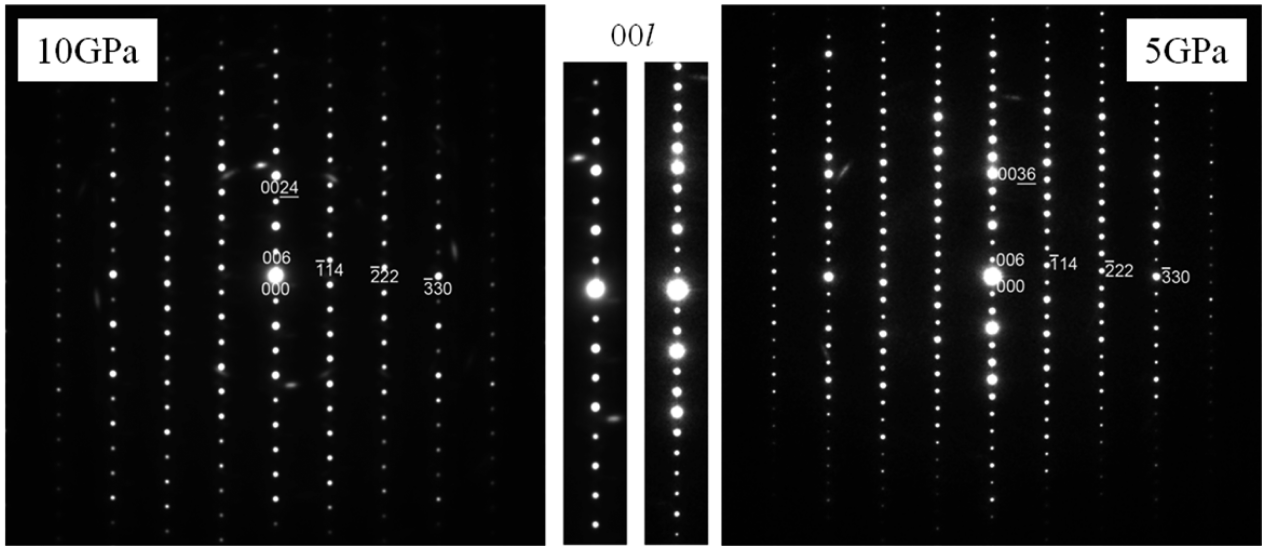

Figure 6. Electron diffraction pattern of $LaPt_5As$ with the beam parallel to the [110] zone axis. Described numbers indicate *hkl* diffraction spot. The center of figures show the spots corresponding to 00*l* to compare the *c* lattice parameters between 5 and 10 GPa.

at 2.6 K under 0 T. It gradually decreases with increasing magnetic field. Also, T_c for each magnetic field was shown in Figure 5b. H_{c2} at 0 K was estimated to be 2 T from the WHH model for a single-band Bardeen–Cooper–Schrieffer (BCS) superconductor: $H_{c2}(0) = 0.69\partial H_{c2}(T)/\partial T|_{T\to T_c}T_c$. In addition, $H_{c2}(0)$ was also predicted from 2.6 to 2 K by fitting to the simple phenomenological expression, $H_{c2}(T) = H_{c2}(0)(1 - (T/T_c)^2)$,[44] to give H_{c2} = 1.6 T at 0 K. To estimate $H_{c2}(0)$ more accurately, superconducting properties at much lower temperature should be investigated. The Ginzburg–Landau coherence length, $\xi_{GL}(0)$, was estimated to be 12.8 nm from the orbital limit of H_{c2} by the Ginzburg–Landau relation, $H_{c2} = \Phi_0/2\pi\xi_{GL}^2(0)$, where Φ_0 is flux quantum. Since this ξ_{GL} is twice the length compared to the *c* lattice parameter of $LaPt_5As$, the

DOI: 10.1021/jacs.6b04976
J. Am. Chem. Soc. 2016, 138, 9927–9934

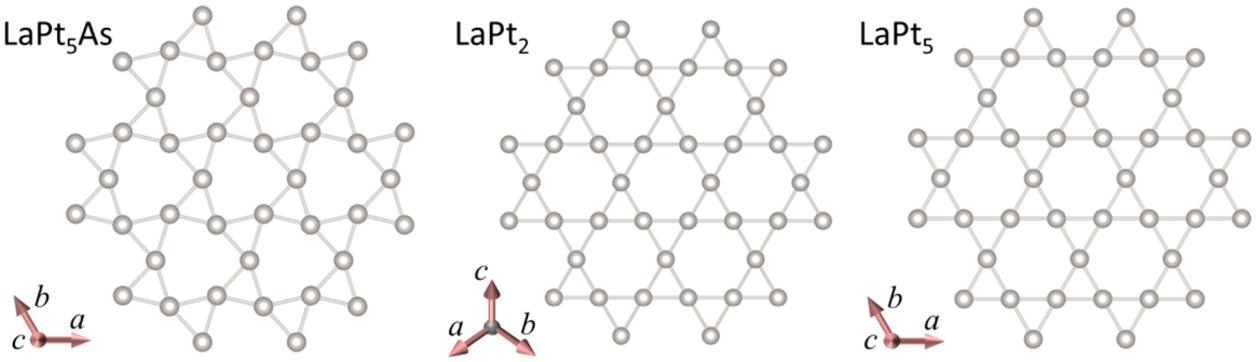

Figure 7. Pt planes for $LaPt_5As$, $LaPt_2$, and $LaPt_5$.

three-dimensional superconductivity is an expected natural occurrence. However, a detailed investigation using single crystals is necessary to discuss the anisotropic properties of $LaPt_5As$. At this stage, single crystalline $LaPt_5As$ has not yet been obtained.

Specific heat is described as $C = \gamma T + \beta/T^3$, where γ is the electronic specific heat coefficient and β is the coefficient of the lattice contribution. The plot of C/T versus T^2 is shown in Figure 5c. From the best fit in a normal conducting state, which is indicated by the black line, the values of $\gamma = 15.46$ mJ/mol·K^2 and $\beta = 9.48$ mJ/mol·K^4 are obtained. The Debye temperature (θ_D) is estimated to be 258 K. Also Pt metal shows an equivalent Debye temperature ($\theta_D = 240$ K). Therefore, lattice specific heat is thought to be mainly dominated by the metallically behaved Pt network of $LaPt_5As$.

The normalized electronic contribution of specific heat ($C_e/\gamma T$) is obtained by $C - \beta/T^3$. The specific heat jump (ΔC_e) at T_c is clearly observed in Figure 5d. $\Delta C_e/\gamma T_c$ is estimated to be 2.2. Such a large value of ΔC_e is evidence of bulk superconductivity for $LaPt_5As$. It is larger than that of the conventional weak coupling of BCS superconductors ($\Delta C_e/\gamma T_c = 1.43$), and also different from that of Pb, which is the typical strong-coupling superconductor ($\Delta C_e/\gamma T_c = 2.77$). Therefore, an intermediate state of weak and strong coupling of BCS was suggested in $LaPt_5As$.

Although, we have also found a phase of $LaPt_5As$ produced at 5 GPa belonging to the same space group as 10 GPa phase ($R\bar{3}c$), the crystal structure has not yet been determined at this stage. However, in comparison to 10 GPa phase, the a lattice parameter is almost the same and 1.5 times as large as the c lattice parameter. This was confirmed by the SAED pattern of the TEM analysis (Figure 6). Corresponding to this large increase in c lattice parameter, the number of atoms in the unit cell of 5 GPa phase is considered to increase up to around 120. For such a large number of atoms, the extrapolation of initial structural model becomes more difficult. Furthermore, the isolation of the 5 GPa phase is difficult to achieve due to the partial formation of the 10 GPa phase, as shown in the Supporting Information (Figure S4). These are the main reasons why we could not determine the crystal structure of the 5 GPa phase. However, at this stage, the XRD patterns of 5 GPa phase have been indexed. The results are displayed in the Supporting Information (Table S2).

Also for the results of the XPS analysis, each binding energy of Pt, La, and As of 5 GPa phase is almost the same as that of 10 GPa phase, as shown in the Supporting Information (Figure S3). In spite of the same oxidation states, space groups, and elemental compositions between the 5 and 10 GPa phases, superconductivity does not appear in the 5 GPa phase. Therefore, the structural differences are thought to hold the key to understanding the superconductivity in these systems.

DISCUSSION

We suggested that the emergence of superconductivity in $LaPt_5As$ is related with its unique crystal structure. To make this point, superconducting $LaPt_2$[40,46] and non-superconducting $LaPt_5$[41,45] were adopted to compare with $LaPt_5As$. These three materials have almost the same Pt−Pt bond length as that of metal Pt and form Pt tetrahedrons also like Pt metal. Therefore, the basic constituents of their structures are very similar in these materials.

Meanwhile, Figure 7 shows that each Pt plane is composed of Pt tetrahedrons. Although the same configurations are observed in $LaPt_2$ and $LaPt_5$, only $LaPt_5As$ shows the unique configuration. Furthermore, Pt tetrahedrons of $LaPt_2$ and $LaPt_5$ spread out three-dimensionally in the crystal structures. However, as described above, $LaPt_5As$ shows the two-dimensional Pt network layers.

As described in the Introduction, large exchange interaction between the itinerant 5d electrons of Pt greatly enhances the spin fluctuations and brings this metal close to a magnetic instability, which competes with the phonon-mediated pairing. This is generally agreed to be the reason why Pt metal does not show superconductivity.[18−24] In regard to the Pt-based superconductors mainly composed of metal-like Pt−Pt bonds, if their crystal structure and physical properties are close to those of Pt metal, it may be worth considering whether the mechanism with the absence of superconductivity in Pt metal is applicable to these materials as well. Actually, $LaPt_2$, $LaPt_5$, $LaPt_5As$, and Pt have the same basic constituents of Pt tetrahedrons.

Table 2 exhibits the electronic state of each material. $LaPt_5$ with a high concentration of 5d electrons (over 80%) at the E_F does not show superconductivity. Conversely, in the case of

Table 2. Comparison of T_c, Pt−Pt Bond Length, and Electronic State at EF for Pt Compounds and Metal[a]

compd	structure	T_c (K)	Pt−Pt bond (Å)	Pt PDOS at EF (%)	Pt 5d PDOS at EF (%)
LaPt2	MgCu2	0.46	2.751	71	41
LaPt5	CaCu5	–	2.68417	97	84
LaPt5As	LaPt5As	2.6	2.71892	92	81
Pt	Cu	–	2.77398	100	98

[a]Each electronic state is calculated by DFT, and the results are shown in the Supporting Information (Figure S6).

DOI: 10.1021/jacs.6b04976
J. Am. Chem. Soc. 2016, 138, 9927−9934

$LaPt_2$, the 5d electron concentration is only 40% at E_F, and superconductivity is observed.

This tendency is also observed in other intermetallic Pt-based superconductors with metal-like Pt−Pt bonds.[45−57] We calculated the electronic states of some compounds using DFT, and also made a list of the different crystal types in the Supporting Information (Table S2). Displayed compounds have exhibited the highest T_c for each crystal type. The results of the calculations are shown in the Supporting Information (Figures S5 and S6). In general, the 5d electron concentration at E_F decreases, and therefore the exchange interaction between the 5d itinerant electrons should also be suppressed. As a result, the spin fluctuations are suppressed, and the material does not exhibit any magnetic instability. Consequently, the enhanced phonon-mediated pairing is expected to induce superconductivity.

However, in these intermetallic Pt-based superconductors, $LaPt_5As$ shows exceptionally high occupancy for the 5d electrons at E_F (over 80%). Such a high 5d electron concentration at the E_F is uncommon. We affirm that the Pt network layers characteristic of $LaPt_5As$ plays a key role in the emergence of its superconductivity. Unlike $LaPt_2$ and $LaPt_5$, Pt network layers in $LaPt_5As$ are spread out two-dimensionally. As shown in Figure 4b,c,e, the stacking structure of $LaPt_5As$ results in large interlayer spacing for every two of the Pt network layers. These spaces are enlarged by the insertion of insulating La1−As layers, whose contributing DOS at the E_F has been neglected. The closest Pt−Pt length across this interlayer space is estimated to be 3.21944 Å. This is much longer than the typical Pt metal bond. This means that the metallic connectivity is broken up along the c axis. Therefore, a 5d orbital overlap should be expected to become smaller along the c axis. These two-dimensional Pt network layers are thought to be effective to suppress the exchange interaction between the itinerant d electron and spin fluctuations, even the 5d electron concentration at the E_F is over 80%. Furthermore, as shown in Figure 7, Pt planes of $LaPt_5As$ show a unique Pt plane. Such an asymmetric crystal field has the possibility to reduce the region of 5d orbital overlap. To ensure this suggestion, although the detailed calculations are required in regard to the configuration of the 5d orbitals, this asymmetric crystal field is also considered as a factor in the suppression of the spin fluctuations of this material.

$LaPt_5As$ is categorized as a BCS superconductor. Therefore, the superconducting transition temperature follows the formula: $T_c \propto \theta_D \exp(-1/N(0)V)$, where θ_D is the Debye temperature, $N(0)$ is the density of electronic state at E_F, and V is the attractive interaction between electrons. The Debye temperature is comparable to those of $LaPt_5As$ and $LaPt_2$ ($LaPt_5As$, θ_D = 256 K; $LaPt_2$, θ_D = 236 K),[58] and the superconducting transition temperature of $LaPt_5As$ is higher than that of $LaPt_2$ ($LaPt_5As$, T_c = 2.6 K; $LaPt_2$, T_c = 0.46 K); therefore, a larger $N(0)V$ is expected for $LaPt_5As$. Concerning the intermetallic Pt-based superconductors, we suggested that the V should be related to the concentration of 5d electrons and their orbital overlap. If we can suppress the interaction of 5d itinerant electrons, T_c is expected to increase in this system.

CONCLUSION

In this research, we discovered the novel Pt-based superconductor $LaPt_5As$ with a unique crystal structure. According to the synthesis pressure, three different crystal structures of $LaPt_5As$ were obtained by the high-pressure synthesis using a Kawai-type apparatus. However, single-phase superconducting $LaPt_5As$ was only obtained under 10 GPa. The crystal structure was determined as hexagonal with space group $R\bar{3}c$ (lattice parameters a = 5. 30633(17) Å, c = 60.7864(14) Å). The corner-sharing tetrahedrons composed of Pt spread in the ab plane with a network-like structure. The DFT calculations suggested that the superconducting current flows through this Pt network. T_c is observed at 2.6 K, and also H_{c2} is estimated to be 2 T based on the WHH model or 1.6 T from the simple phenomenological expression. Bulk superconductivity is observed from the heat-specific measurement. The value of $\Delta C_e/\gamma T_c$ is not explained by the conventional weak coupling of BCS superconductors. The oxidation state of each element, space group, and elemental composition are almost the same between the 5 and 10 GPa phases. However, superconductivity is observed only in the 10 GPa phase. So, determination of the detailed crystal structure of the non-superconducting $LaPt_5As$ would aid our understanding of the emergence of superconductivity. In fact, from the comparison of the intermetallic Pt-based compounds with Pt−Pt metal-like bonds, we suggest that the Pt network layers, characteristic of the $LaPt_5As$, plays a key role in the emergence of its superconductivity. This structure possibly reduces the region of 5d orbital overlap and suppresses the interactions between the 5d itinerant electrons and spin fluctuations. Therefore, the enhanced phonon-mediated pairing is expected to induce superconductivity in $LaPt_5As$.

ASSOCIATED CONTENT

Supporting Information

The Supporting Information is available free of charge on the ACS Publications website at DOI: 10.1021/jacs.6b04976.

Space group determination for 10 GPa phase; XPS measurements for 5 and 10 GPa; synchrotron XRD measurements for 5 GPa phase; DFT calculations for intermetallic Pt-based superconductors (PDF)

AUTHOR INFORMATION

Corresponding Author

*fujioka@es.hokudai.ac.jp

Notes

The authors declare no competing financial interest.

ACKNOWLEDGMENTS

This research has been partially supported by a Grant-in-Aid for Yang Scientists from the Japan Society for the Promotion of Science (JSPS; Grant No. 15K17711), Nanotech Career-up Alliance (CUPAL), and the Cooperative Research Program of the Network Joint Research Center for Materials and Devices from the Ministry of Education, Culture, Sports, Science and Technology (MEXT). The authors thank Dr. Y. Mizuguchi (Tokyo Metropolitan University) for the experimental help with synchrotron X-ray powder diffraction measurements (JASRI; Proposal 2015A1441) and Dr. S. J. Denholme (Tokyo University of Science) for proofreading of the manuscript.

REFERENCES

(1) Raub, C. J. *Platinum Met. Rev.* **1984**, *28*, 63−75.
(2) Ivanovskii, A. L. *Platinum Met. Rev.* **2013**, *57*, 87−100.
(3) Joynt, R.; Taillefer, L. *Rev. Mod. Phys.* **2002**, *74*, 235−294.

DOI: 10.1021/jacs.6b04976
J. Am. Chem. Soc. 2016, 138, 9927−9934

(4) Bauer, E.; Hilscher, G.; Michor, H.; Paul, Ch.; Scheidt, E. W.; Gribanov, A.; Seropegin, Yu.; Noël, H.; Sigrist, M.; Rogl, P. *Phys. Rev. Lett.* **2004**, *92*, 027003.
(5) Bauer, E.; Khan, R. T.; Michor, H.; Royanian, E.; Grytsiv, A.; Melnychenko-Koblyuk, N.; Rogl, P.; Reith, D.; Podloucky, R.; Scheidt, E.-W.; Wolf, W.; Marsman, M. *Phys. Rev. B: Condens. Matter Mater. Phys.* **2009**, *80*, 064504.
(6) Samokhin, K. V.; Mineev, V. P. *Phys. Rev. B: Condens. Matter Mater. Phys.* **2008**, *77*, 104520.
(7) Aoki, Y.; Sumiyama, A.; Shiotsuki, M.; Motoyama, G.; Yamaguchi, A.; Oda, Y.; Yasuda, T.; Settai, R.; Ōnuki, Y. *J. Phys. Soc. Jpn.* **2010**, *79*, 124707.
(8) Cava, R. J.; Batlogg, B.; Siegrist, T.; Krajewski, J. J.; Peck, W. F., Jr.; Carter, S.; Felder, R. J.; Takagi, H.; van Dover, R. B. *Phys. Rev. B: Condens. Matter Mater. Phys.* **1994**, *49*, 12384.
(9) Paulose, P. L.; Dhar, S. K.; Chinchure, A. D.; Alleno, E.; Godart, C.; Gupta, L. C.; Nagarajan, R. *Phys. C* **2003**, *399*, 165.
(10) Takabatake, T.; Maeda, Y.; Konishi, T.; Fujii, H. *J. Phys. Soc. Jpn.* **1994**, *63*, 2853.
(11) Jeng, F. S.; You, Y. B.; Ku, H. C.; Ho, J. C. *Phys. Rev. B: Condens. Matter Mater. Phys.* **1996**, *53*, 3492.
(12) Takayama, T.; Kuwano, K.; Hirai, D.; Katsura, Y.; Yamamoto, A.; Takagi, H. *Phys. Rev. Lett.* **2012**, *108*, 237001.
(13) Kakiya, S.; Kudo, K.; Nishikubo, Y.; Oku, K.; Nishibori, E.; Sawa, H.; Yamamoto, T.; Nozaka, T.; Nohara, M. *J. Phys. Soc. Jpn.* **2011**, *80*, 093704.
(14) Ni, N.; Allred, J. M.; Chan, B. C.; Cava, R. J. *Proc. Natl. Acad. Sci. U. S. A.* **2011**, *108*, E1019.
(15) Löhnert, C.; Stürzer, T.; Tegel, M.; Frankovsky, R.; Friederichs, G.; Johrendt, D. *Angew. Chem., Int. Ed.* **2011**, *50*, 9195.
(16) Wendler, W.; Herrmannsdörfer, T.; Rehmann, S.; Pobell, F. *Europhys. Lett.* **1997**, *38*, 619.
(17) Webb, R. A.; Ketterson, J. B.; Halperin, W. P.; Vuillemin, J. J.; Sandesara, N. B. *J. Low Temp. Phys.* **1978**, *32*, 659−664.
(18) Katayama, D.; Sumiyama, A.; Oda, Y. *Phys. Rev. B: Condens. Matter Mater. Phys.* **2003**, *68*, 132502.
(19) Fay, D.; Appel, J. *Phys. Rev. Lett.* **2002**, *89*, 127001.
(20) Andres, K.; Jensen, M. A. *Phys. Rev.* **1968**, *165*, 533.
(21) Jensen, M. A.; Andres, K. *Phys. Rev.* **1968**, *165*, 545.
(22) Fradin, F. M.; Koelling, D. D.; Freeman, A. J.; Watson-Yang, T. J. *Phys. Rev. B* **1975**, *12*, 5570.
(23) Berk, N. F.; Schrieffer, J. S. *Phys. Rev. Lett.* **1966**, *17*, 433.
(24) Herrmannsdörfer, T.; Rehmann, S.; Wendler, W.; Pobell, F. *J. Low Temp. Phys.* **1996**, *104*, 49.
(25) Schindler, A.; König, R.; Herrmannsdörfer, T.; Braun, H. F.; Eska, G.; Günther, D.; Meissner, M.; Mertig, M.; Wahl, R.; Pompe, W. *Phys. B: Condens. Matter* **2003**, *329*−*333*, 1427.
(26) König, R.; Schindler, A.; Herrmannsdörfer, T. *Phys. Rev. Lett.* **1999**, *82*, 4528.
(27) Schindler, A.; König, R.; Herrmannsdörfer, T.; Braun, H. F. *Phys. Rev. B: Condens. Matter Mater. Phys.* **2000**, *62*, 14350.
(28) van Leeuwen, D. A.; van Ruitenbeek, J. M.; Schmid, G.; de Jongh, L. J. *Phys. B* **1994**, *194*−*196*, 263−264.
(29) Bednorz, J. G.; Muller, K. A. *Z. Phys. B: Condens. Matter* **1986**, *64*, 189.
(30) Kamihara, Y.; Watanabe, T.; Hirano, M.; Hosono, H. *J. Am. Chem. Soc.* **2008**, *130*, 3296.
(31) Fujioka, M.; Denholme, S. J.; Tanaka, M.; Takeya, H.; Yamaguchi, T.; Takano, Y. *Appl. Phys. Lett.* **2014**, *105*, 102602.
(32) Mizuguchi, Y.; Fujihisa, H.; Gotoh, Y.; Suzuki, K.; Usui, H.; Kuroki, K.; Demura, S.; Takano, Y.; Izawa, H.; Miura, O. *Phys. Rev. B: Condens. Matter Mater. Phys.* **2012**, *86*, 220510.
(33) Fujioka, M.; Nagao, M.; Denholme, S. J.; Tanaka, M.; Takeya, H.; Yamaguchi; Takano, Y. *Appl. Phys. Lett.* **2014**, *105*, 052601.
(34) Kawai, N.; Endo, S. *Rev. Sci. Instrum.* **1970**, *41*, 1178.
(35) Altomare, A.; Cuocci, C.; Giacovazzo, C.; Moliterni, A.; Rizzi, R.; Corriero, N.; Falcicchio, A. *J. Appl. Crystallogr.* **2013**, *46*, 1231−1235.
(36) Izumi, F.; Momma, K. *Solid State Phenom.* **2007**, *130*, 15.
(37) Perdew, J. P.; Burke, K.; Ernzerhof, M. *Phys. Rev. Lett.* **1996**, *77*, 3865−3868.
(38) Kresse, G.; Hafner, J. *Phys. Rev. B: Condens. Matter Mater. Phys.* **1993**, *47*, 558−561.
(39) Kresse, G.; Furthmüller, J. *Phys. Rev. B: Condens. Matter Mater. Phys.* **1996**, *54*, 11169−11186.
(40) Erdmann, B.; Keller, C. *J. Solid State Chem.* **1973**, *7*, 40.
(41) Ning, Y. T.; Zhou, X. M.; Zhen, Y.; Chen, N. Y.; Xu, H.; Zhu, J. Z. *J. Less-Common Met.* **1989**, *147*, 167.
(42) Bahn, S. R.; Jacobsen, K. W. *Comput. Sci. Eng.* **2002**, *4*, 56.
(43) Nagano; Tomioka, Y.; Nakayama, Y.; Kishio, K.; Kitazawa, K. *Phys. Rev. B: Condens. Matter Mater. Phys.* **1993**, *48*, 9689.
(44) Gorter, C.; Casimir, H. *Phys. Z.* **1934**, *35*, 963−969. Kresse, G.; Hafner, J. *Phys. Rev. B: Condens. Matter Mater. Phys.* **1993**, *47*, 558−561.
(45) Matthias, B. T.; Corenzwit, E.; Hull, G. W.; Longinotti, L. D., Jr.; Geballe, T. H.; Compton, V. B. *Phys. Rev.* **1965**, *137*, A119.
(46) Bronger, W. *J. Less-Common Met.* **1967**, *12*, 63.
(47) Krannich, S.; Lamago, D.; Manske, D.; Bauer, E.; Prokofiev, A.; Heid, R.; Bohnen, K.-p.; Weber, F. *Phys. Rev. B: Condens. Matter Mater. Phys.* **2015**, *92*, 125137.
(48) Jung, M.-C.; Kang, C.-J.; Min, B. I.; Lee, K.-W. *Phys. Rev. B: Condens. Matter Mater. Phys.* **2013**, *87*, 144509.
(49) Singh, D. J. *Phys. Rev. B: Condens. Matter Mater. Phys.* **1994**, *50*, 6486.
(50) Albers, R. C.; Boring, A. M.; Christensen, N. E. *Phys. Rev. B: Condens. Matter Mater. Phys.* **1986**, *33*, 8116.
(51) Nekrasov, I. A.; Sadovskii, M. V. *JETP Lett.* **2012**, *96*, 227.
(52) Chandra, S.; Jaya, S. M.; Valsakumar, M. C. *Phys. C* **2005**, *432*, 116.
(53) Zhuravlev, N. N.; Zhdanov, G. S.; Smirnova, Y. M. *Phys. Met. Metallogr.* **1962**, *13*, 55.
(54) Pfisterer, H.; Schubert, K. *Z. Metallkd.* **1950**, *41*, 358.
(55) Havinga, E. E.; Damsma, H.; Hokkeling, P. *J. Less-Common Met.* **1972**, *27*, 169.
(56) Compton, V. B.; Matthias, B. T. *Acta Crystallogr.* **1959**, *12*, 651.
(57) Li, S.; Xing, J.; Tao, J.; Yang, H.; Wen, H.-H. *Ann. Phys.* **2015**, *358*, 248.
(58) Joseph, R. R.; Gschneidner, K. A., Jr. *Scr. Metall.* **1968**, *2*, 631.

DOI: 10.1021/jacs.6b04976
J. Am. Chem. Soc. 2016, 138, 9927−9934